PFC/JA–90–13

Velocity Ratio Measurements of a Gyrotron Electron Beam

Guss, W.C.; Grimm, T.L.; Kreischer, K.E.
Polevoy, J.T.; Temkin, R.J.

Plasma Fusion Center
Massachusetts Institute of Technology
Cambridge, MA 02139

April 1990

This work was supported by U.S. D.O.E. Contract DE–AC02–78ET51013.

Velocity Ratio Measurements of a Gyrotron Electron Beam

W.C. Guss, T.L. Grimm, K.E. Kreischer,
J.T. Polevoy, and R.J. Temkin

Plasma Fusion Center, MIT

Abstract

A 140 GHz high power gyrotron has recently been operated in a 14 T Bitter magnet to characterize emission as a function of magnetic field and beam current. The velocity ratio (or pitch angle) $\alpha = \langle v_\perp \rangle / \langle v_{||} \rangle$ of the beam electrons is a critical parameter for high efficiency gyrotron operation and was measured using a capacitive probe located in the beam tunnel before the cavity. The observed velocity ratio decreased as the beam current increased while the beam voltage and magnetic fields were held fixed. This decrease in α partially explains the reduced gyrotron efficiency observed at high beam currents. The velocity ratio exhibited saturation effects as a function of both the beam current and the control-anode voltage, at low cathode magnetic field values. Particle code results show a decrease in α as a function of beam current that is consistent in magnitude with the observed values.

I. Introduction

Recent attempts at increasing emitted power from a 140 GHz gyrotron have shown differences between theoretical efficiency predictions and observed values particularly at larger values of beam current[1]. While at beam current levels less than ≈ 20 A efficiencies agree with theoretical expectations, at 80 kV and 35 A, a maximum power of 645 kW was measured for an efficiency of 23%, compared with a theoretical prediction of 1.3 MW at an efficiency of 46%. A peak power of 925 kW was measured at 120 kV and 40 A, but with efficiency of only 19%. Several cavities of different lengths, and cavity quality factors Q, were investigated with substantially the same result, suggesting that a beam related parameter may be important. For instance, nonlinear theory[2] and computations[3] indicate that the emitted microwave power is strongly dependent on the velocity ratio, $\alpha = \beta_\perp/\beta_{||}$ and perpendicular velocity spread $\delta\beta_\perp/\beta_\perp$, where $\beta = v/c$ with v and c the electron velocity and the speed of light respectively, and the parallel $||$ and perpendicular $\perp$ components are with respect to the local magnetic field. The previous theoretical predictions assumed that α was a constant equal to the electron gun design value and was not a function of the beam current.

A diagnostic was added to the gyrotron to determine whether α reached its expected value or whether it changed as a function of some parameter, *e.g.* beam current. Capacitive probes were selected for the velocity ratio measurement because they do not perturb the electron beam allowing simultaneous power measurements to be made. Normal operation of the gyrotron is preserved as a result. The probes actually measure beam electron density, from which the average $\beta_{||}$ of the electrons can be determined. With a knowledge of the electron energy, the average velocity ratio can be calculated. The probes have been used by several researchers[4,5] to measure electron beams in free electron lasers. We report on the first use of these probes in a gyrotron and their use in determining the velocity ratio as well as the streaming velocity.

The remainder of the paper is organized as follows. In Section II, we describe the electron gun and the capacitive probe. Section III contains the experimental results which are then discussed in Section IV in the context of several explanations for the observed discrepancies with predictions. The candidates can be catagorized into cavity effects, in particular, mode competition, beam effects which include beam quality and velocity ratio, beam optics, which includes space charge, and beam instabilities. Conclusions are presented in

Section V.

II. Experimental Apparatus

The electron beam was generated by a magnetron injection gun (MIG) source in a 140 GHz high power gyrotron. A schematic of the gun and gyrotron is contained in Fig. 1. The cavity magnetic field is produced by a copper Bitter coil magnet that produces fields up to 14 T. The electron gun was designed[6] to operate at 80 kV and 35 A with $\alpha = 1.93$ at a control-anode voltage of 25.2 kV, however it has been operated at voltages as high as 120 kV with currents as high as 45 A. The computed velocity spread was $\delta v_\perp / v_\perp = \pm 4\%$ under standard conditions. In the cavity, the beam radius is $r_b = 0.53\ cm$. The cavity has a radius $r_c = 0.75\ cm$ and length $L_c = 1.28\ cm$ ($L_c/\lambda_o = 6.0$, where L is determined from a self-consistent Gaussian field profile, and λ_o is the free-space wavelength). The cavity was designed to resonate with the $TE_{15,2,1}$ mode at 140 GHz. and has also been operated successfully[7] in other modes including the $TE_{16,2,1}$ mode at 148 GHz. The control-anode voltage during 80 kV operation was $24.5 - 25.0\ kV$. The pulse length was $1 - 3\ \mu s$. The limiting beam current[8], I_{lim}, is the maximum beam current for a given velocity ratio α, beam radius, and cavity radius, that will propagate, subject to the effects of space charge. For our parameters, as listed above, I_{lim} is predicted to be about 69 A.

To determine whether the design α was achieved, a capacitive probe was installed. The probe directly measures ξ, the charge density per unit beam length, by the voltage induced between the two concentric cylindrical electrodes. After determination of the total beam current $I_b = \xi \langle v_{||} \rangle$, the parallel velocity $\langle v_{||} \rangle$ can be found.

For purposes of illustration of their operation, the probe geometry can be idealized as two thin concentric cylindrical electrodes which have an electron beam along the axis. We assume that their length is large compared to their radius. First, we note that the beam electrons passing through the capacitive probe induce a charge on the inner electrode which appears as a voltage difference V_p between the electrodes. Gauss' Law gives the electric field, E_r, between the electrodes for a beam with volume charge density ρ,

$$\int E_r \, r d\phi dz = \frac{-1}{\epsilon} \int \rho \, r d\phi dr dz \ ,$$

or

$$2\pi r E_r = \frac{-\xi}{\epsilon} .$$

where $\xi = \int \rho \, r d\phi dr$ and ϵ is the dielectric constant in the interstitial space. Then the voltage between the electrodes is

$$\begin{aligned} V_p &= -\int_{r_i}^{r_o} E_r \, dr \\ &= \frac{\xi}{2\pi\epsilon} ln\,(r_o/r_i) \\ &= \frac{\xi}{C_p} . \end{aligned}$$

where C_p is the inter-electrode capacitance per unit length and is given by

$$C_p = \frac{2\pi\epsilon}{ln\left(\frac{r_o}{r_i}\right)} , \tag{1}$$

where r_i and r_o are the inner electrode and outer electrode radius respectively. With the exception of ξ all the variables in this equation are known, and ξ is determined by noting that at the axial location of the probe, $I_b = \langle v_{\|} \rangle \xi$. Then

$$\begin{aligned} \langle v_{\|} \rangle &= \frac{I_b}{\xi} \\ &= \frac{I_b}{C_p V_p} . \end{aligned}$$

Consequently,

$$\langle v_{\|} \rangle = \frac{I_b}{2\pi\epsilon V_p} ln\left(\frac{r_o}{r_i}\right) . \tag{2}$$

Experimentally, the beam current is determined at the gyrotron collector rather than under the probe cylinders. Except for the case of significant beam interception, the current at both locations is the same.

Once the parallel velocity is measured, the perpendicular velocity can be estimated assuming the cathode voltage determines the electron energy, and $\gamma = (1-\beta_{||}^2-\beta_{\perp}^2)^{-1/2}$. A refinement to the expression for γ includes the voltage depression of the beam at the probe location. For an ideal cylindrical geometry which approximates the beam tunnel geometry, the voltage depression for a thin annular beam is given by[9]

$$\delta V \approx \frac{I_b}{2\pi\epsilon\langle v_{||}\rangle} ln\left(\frac{r_w}{r_b}\right) ,$$

where r_w, r_b are the wall and beam radius respectively. Then

$$\langle\beta_{\perp}\rangle = \sqrt{1 - \frac{1}{\gamma'^2} - \langle\beta_{||}\rangle^2}$$

with

$$\gamma' = 1 + \frac{e(V_c - \delta V)}{m_o c^2}$$

where V_c is the cathode or accelerating voltage. Typically the voltage depression is less than 5 kV in our experiments. The value of $\langle v_{||}\rangle$ has only a weak dependence on the beam radius, which may vary with operating conditions, through the logarithmic factor in the voltage correction term. Finally, the velocity ratio $\langle\alpha\rangle = \langle v_{\perp}\rangle/\langle v_{||}\rangle$ can be determined. Our use of the capacitive probe is different than previous workers[4,5] in the determination of the velocity ratio and the inclusion of an estimate of the voltage depression.

The actual probe location and geometry is shown in Fig. 2. A sample output of the beam current and probe voltage is shown in Figs. 3 and 4. A high impedence scope probe is attached to the capacitive probe to ensure that $RC >> 1$, where C is the capacitance-probe capacitance and R is the probe plus cable resistance, for proper operation. The probe voltage is typically $25 - 35$ V for a beam current of ≈ 30 A, and has the same signature as that of the beam current. The probe voltage range is a result of different α values.

The actual probe geometry is not reflected in the idealized model discussed earlier. Stray capacitance, cylindrical asymmetries and other nonidealizations are not part of the model. Rather than develop an involved analytic or computational model to include realistic physical parameters and geometry, a calibration procedure was chosen. One method is to measure *in situ*

the capacitance and utilize some of the above equations. Another more direct calibration involves placing a metal tube on the gyrotron axis to simulate the electron beam. The tube is then connected to the same high voltage supply used to bias the cathode, and pulsed to a moderate voltage. The results of this procedure are shown in Fig. 5. The probe voltage scales linearly as expected. Finally, the gyrotron was used for a rough calibration by reducing the perpendicular electron velocity so that $v_{||} \approx v$ where v is determined directly from the accelerating voltage. These operating conditions were realized by reducing the magnetic field ratio between cathode and cavity, and by reducing the control-anode voltage. The tube calibration and the operational method based on low $v_{\perp}$ operation were compared, and found to agree to $\approx 7\%$.

In addition to the calibration uncertainty, there are uncertainties in determining the probe voltage, the beam voltage and current giving a total error in the velocity ratio measurement of about 10% for $\alpha \geq 2$, and increasing to about 20% at $\alpha = 1$.

III. Results

Figure 6 shows the gyrotron efficiency given by theory and experiment. The theoretical curve was obtained using a nonlinear, self-consistent computer code[10] using at each beam current value, the velocity ratio value ($\alpha = 1.93$) from the gun design, and the beam voltage ($80\ kV$) typical for our gyrotron operation. Velocity spread was not included in the calculation. The theory shows good agreement with experiment for beam currents below $\approx 15\ A$ then diverges from the experimental values at larger currents. The difference at $35\ A$ is a factor of two which can not be explained by the absence of velocity spread in the theory model. At the reduced efficiency for beam currents of $35 - 40\ A$, the output power is $\approx 0.75\ MW$; with a modest improvement in efficiency, powers in excess of $1\ MW$, the design goal, would be possible.

The capacitive probe provided some added information to explain the discrepancy. Figure 7 shows the velocity components $\beta_{||}$ and $\beta_{\perp}$ for gyrotron operation in the $TE_{15,2}$ mode. The values of $\beta_{||}$ were measured directly by the capacitive probe, and the values of $\beta_{\perp}$ were derived from $\beta_{||}$ with voltage depression corrections. The change in $\beta_{||}$ from $20\ A$ to $40\ A$ is 34% and for $\beta_{\perp}$ it is 13%. Figure 8 shows the ratio of the experimental velocity components of the previous figure, as a function of the beam current for a fixed control-anode voltage and optimized cavity magnetic field. Velocity ratio values for

beam currents $\leq 20\ A$ are relatively constant and for currents $\geq 20\ A$ the velocity ratio shows a linear decrease. Figure 9 shows the measured α values, from the probe for a range of beam current values. Also included is a curve showing the α dependence on magnetic field as given by adiabatic theory. From conservation of magnetic moment

$$\beta_\perp = \left(\frac{E_{g\perp}}{cB_g}\right)\sqrt{\frac{B_o}{B_g}}\ ,$$

where E_g, and B_g are the electric and magnetic fields at the cathode. Then

$$\alpha = \left(\frac{\gamma^2 - 1}{\gamma^2\beta_\perp^2} - 1\right)^{-1/2}\ .$$

The general behavior of the experimental velocity ratio is consistent with adiabatic theory however the experimental α values have a much stronger cathode magnetic field dependence than was predicted by the simple adiabatic equations. Two additional conclusions come from this data. First, at low cathode field (high compression), the α values for all current levels saturate. It also appears that the higher beam currents show this effect at lower compression than the lower beam currents. Second, the saturation values of α are a function of beam current with the higher beam currents having smaller α values. While the cathode magnetic field varies slightly for the various beam current values when operating at high efficiency output, it is approximately constant and corresponds to a vertical slice in Fig. 9.

A particle trajectory code[11] was used to model the experimental conditions. The code includes the magnet coil locations and currents to model the external magnetic field, as well as space charge and relativistic effects. It also includes the beam self magnetic fields. For the gun geometry and the appropriate beam parameters, α values were generated and compared to the measured values (Fig. 10). Operating parameters in this case were $B_o = 56.0\ kG$, $V_c = 80\ kV$, and $V_a = 25.15\ kV$, for the cavity field, the beam voltage and the control-anode voltage respectively. A beam current of $20\ A$ was selected which displays the α saturation effect (Fig. 9). Agreement between the experimental and computational points is good for lower compresssion values (large cathode magnetic fields). Experimentally low values of cathode magnetic field (high compression) were inaccessible because of arcing and consequently were not studied computationally. Typical operating

points for each beam current were at the lowest cathode field values. At larger compression values, the computational points do not show saturation.

Knowing that the α values are not constant as a function of beam current as had been previously assumed, new theoretical estimates of the efficiency can be computed, and are shown in Fig. 6. With the experimentally determined α values the theoretical efficiencies with zero velocity spread decrease significantly in magnitude. The magnitude however is still larger than the experimentally observed efficiencies.

The effects of velocity spread were modeled with additional computations using a self-consistent, nonlinear code with a Gaussian distribution of electron velocities. Efficiencies were calculated for $\alpha = 1.93$ and several perpendicular velocity spreads between zero and $\pm 7.5\%$, and are shown in Fig. 11 as a function of cavity magnetic field. At the magnetic field in the range of $57\ kG$, the $\pm 7.5\%$ velocity spread can have $\approx 10\%$ lower efficiency than the zero velocity spread case. Similar results are expected at the lower α values observed in the gyrotron. At present, no measurements of the velocity spread are available. However, for a beam current of $35\ A$, the gun is estimated[6] to have a velocity spread of $\delta v_\perp / v_\perp \approx \pm 4\%$ at the cavity implying that there is perhaps a 5% efficiency decrease. It is also estimated to be relatively independent of the control-anode voltage. Upper bounds for the perpendicular velocity spread can be estimated by assuming that the constancy of the electron energy, and the limiting spread in the parallel velocity. Using the invariance of the energy we find

$$\frac{\delta v_\perp}{v_\perp} = \frac{1}{\alpha^2} \frac{\delta v_\parallel}{v_\parallel} \ .$$

The maximum parallel velocity spread occurs for electrons which are about to turn back to the cathode, perhaps because the cathode magnetic field is sufficiently small, and have $\delta v_\parallel / v_\parallel \approx 1/2$. Then $\delta v_\perp / v_\perp \leq (2\alpha^2)^{-1}$. For the design value of $\alpha = 1.93$, the maximum perpendicular velocity spread is $\approx \pm 12\%$, and for a lower value of the experimentally observed velocity ratio, $\alpha = 1.35$, the maximum velocity spread is about $\pm 27\%$.

IV. Discussion

Now it is possible to compare the experimental results to the computational expectations. From Fig. 6, the difference between the computational

and the experimental curve for constant $\alpha = 1.93$ is about 26% at a beam current of 35 A. Adding the observed α values decreases the difference to about 15%, and adding an estimated velocity spread effect further decreases the discrepancy to about 10%. Experimental error in the velocity ratio is not large enough to account for this magnitude, however there is a large uncertainty in the velocity spread.

The discrepancy between the constant α efficiency calculations and the experimental results has been shown to be largely a result of a current dependent α and velocity spread. There remains the question of why the velocity ratio is different from the design value. There are a number of phenomena that can affect properties of the electron beam and thus affect the efficiency of microwave emission. Some of these phenomena require experimental identification to meaningfully assess their impact on the beam. Mode competition and beam instabilities fall into this category. On the other hand, DC space charge effects, such as voltage depression, are expected to be present because of the mere presence of the beam electrons and have quantifiable effects that are already known analytically. As a result, they can be included as a zeroth order correction and any remaining discrepancies can be examined with respect to mode competition and beam instabilities. DC space charge effects were purported to have been taken into account during the design of the gun in such a way that the design α could be attained at higher beam currents with low perpendicular velocity spread.

Space charge effects become important as the electron density, and thus electron current, increase. Space charge has the two DC effects[9] of increasing the velocity spread radially across the beam as a result of potential differences across the beam, and increasing the potential between the beam and any nearby conductor. The former effect should be largest where the potential gradient across the beam is largest, specifically in the gun. It causes a deterioration of the beam quality and hence efficiency. Neilson, *et al.*[12] have also shown computationally that space charge increases the velocity spread on beams generated by MIG and Pierce-wiggler sources. Space charge effects in locations other than the gun region have been theoretically shown[13] to also produce velocity spread. The latter effect, beam-wall potentials, can occur in several places. In the gun, space charge decreases the cathode to control-anode potential decreasing the local $v_\perp$. An estimate of the decrease in α with space charge voltage was obtained by purposely varying the control-anode voltage which also changes the voltage gradient at the beam. Figure 12 shows the experimental behavior of

the velocity ratio by varying the control-anode voltage. While there is some change in α at higher cathode magnetic field (lower compression), at the lower values of cathode magnetic field, the α values saturate much as they did as a function of current. In the moderate compression region of interest, larger control-anode voltages would be required to obtain the design α. The other location where space charge effects are important is at the cavity. Here, however the voltage depression serves to decrease $\beta_{||}$ and thus increases α. This is not the tendency observed experimentally except when the beam electrons mirror. Currents for which this would be a strong effect are near the limiting current I_{lim} which is larger than the values encountered in the experiment. Space charge can also have ac effects which affect bunching. We operate at current densities that are sufficiently small that ac effects are small[13].

Conclusions

Operation of the high power 140 GHz gyrotron yielded efficiencies that are somewhat lower than predicted from self-consistent nonlinear computations. A capacitive probe provided information that the electron velocity ratio varied as a function of beam current and was not as large as the design value ($\alpha = 1.93$) above 15 A. The observed α measurements showed an approximately linear decrease with increasing beam current above 20 A. The linear behavior of the measured α values is suggestive of space charge effects. Probe measurements also show a saturation in α with decreasing cathode field $i.e.$ with higher compression. Computations which include space charge effects in the electron gun, produce velocity ratios generally in agreement with experiment for low to moderate values of α. When the experimentally determined velocity ratios are used to computationally predict the efficiency using a model of zero velocity spread, discrepancies with observed effiencies still exist. Inclusion of velocity spread to the computational efficiencies reduces but does not eliminate the discrepancy unless the perpendicular velocity spread is much larger than expected.

Acknowledgements

This research is supported by the Department of Energy Contract DE-AC02-78ET51013. Parts of this experimental program were conducted using the facilities at the Francis Bitter National Magnet Laboratory, Cambridge, MA. We also gratefully acknowledge the assistance of W. Mulligan, G. Yarworth, and K. Xu.

References

[1] K.E. Kreischer, T.L. Grimm, W.C. Guss, A.W. Mobius, and R.J. Temkin, Phys. Fluids B **2**, 640(1990)

[2] B.G. Danly, and R.J. Temkin, Phys. Fluids **29**, 561(1986)

[3] M. Caplan, A.T. Lin, and K.R. Chu, Int. J. Electronics **53**, 659(1982)

[4] P. Avivi, Ch. Cohen, and L. Friedland, Appl. Phys. Lett. **42**, 948(1983)

[5] R.E. Shefer, Y.Z. Yin, and G. Bekefi, J. Appl. Phys. **54**, 6154(1983)

[6] H. Huey, N. Lopez, R. Garcia, K.E. Kreischer, *Tenth International Conference on Infrared and Millimeter Waves*, p.223 (1985)

[7] K.E. Kreischer, and R.J. Temkin, Phys. Rev. Lett. **57**, 547(1987)

[8] A.K. Ganguly, and K.R. Chu, Int. J. Infrared Millimeter Waves **5**, 103 (1984)

[9] A.T. Drobot, and K. Kim, Int. J. Electronics **51**, 351(1981)

[10] A. Fliflet, M. Read, K. Chu, and R. Seeley, Int. J. Electronics **53**, 505 (1982)

[11] W.B. Herrmannsfeldt, Electron Trajectory Program, SLAC 226, Stanford Linear Accelerator Center, Stanford, CA 94305, November 1979.

[12] J. Neilson, M. Caplan, N. Lopez, K.Felch, International Electron Devices Meeting Technical Digest, p.184 (1985)

[13] Thomas M. Antonson, Wallace M. Manheimer, and Baruch Levush, Int. J. Electronics **61**, 823(1986)

Figure Captions

Figure 1. The 140 GHz megawatt gyrotron. The cavity magnetic field is produced by a 14 T copper Bitter magnet.

Figure 2. The second beam scraper section before the cavity entrance was machined down to form the floating plate of the capacitance probe. The beam tunnel outer wall was the ground plate.

Figure 3. Typical cathode voltage (a), 25 kV/div, and beam current (b), 10 A/div. The time scale is 0.5 $\mu s/div$.

Figure 4. Capacitive probe signal after a $10x$ voltage probe (a), $1V/div$, and beam current (b), $10A/div$. The time scale is 0.5 $\mu s/div$.

Figure 5. Capacitive probe voltage as a function of bias voltage on a metal tube inserted along the gyrotron axis.

Figure 6. Theoretical estimates for the gyrotron efficiency were made using nonlinear self-consistent computations assuming the design value $\alpha = 1.93$, and zero velocity spread. The experimental points are for 80 kV operation in the $TE_{15,2}$ mode.

Figure 7. Velocity components $\beta_{||}$ and $\beta_{\perp}$ as a function of beam current for the $TE_{15,2}$ mode. The anode voltage was 80 kV, and the relative control-anode voltage was 25.1 kV.

Figure 8. Measured α as a function of beam current for the $TE_{15,2}$ mode. Cathode and cavity magnetic fields were optimized for maximum ouput power at each beam current.

Figure 9. The velocity ratio α versus cathode magnetic field for several values of beam current. The beam voltage and cavity magnetic field values were held constant for the entire scan. Typical values of cathode magnetic field for gyrotron operation are in the saturated region. The dashed line is the α predicted from adiabatic theory.

Figure 10. Computational values of α compared to the experimentally measured values for $I_b = 20$ A.

Figure 11. Efficiency for several typical values of velocity spread for gyrotron operation (80 $kV, 35$ A) versus cavity magnetic field.

Figure 12. Measured velocity ratio for several control-anode voltages as a function of cathode magnetic field.

SCHEMATIC OF EXPERIMENT

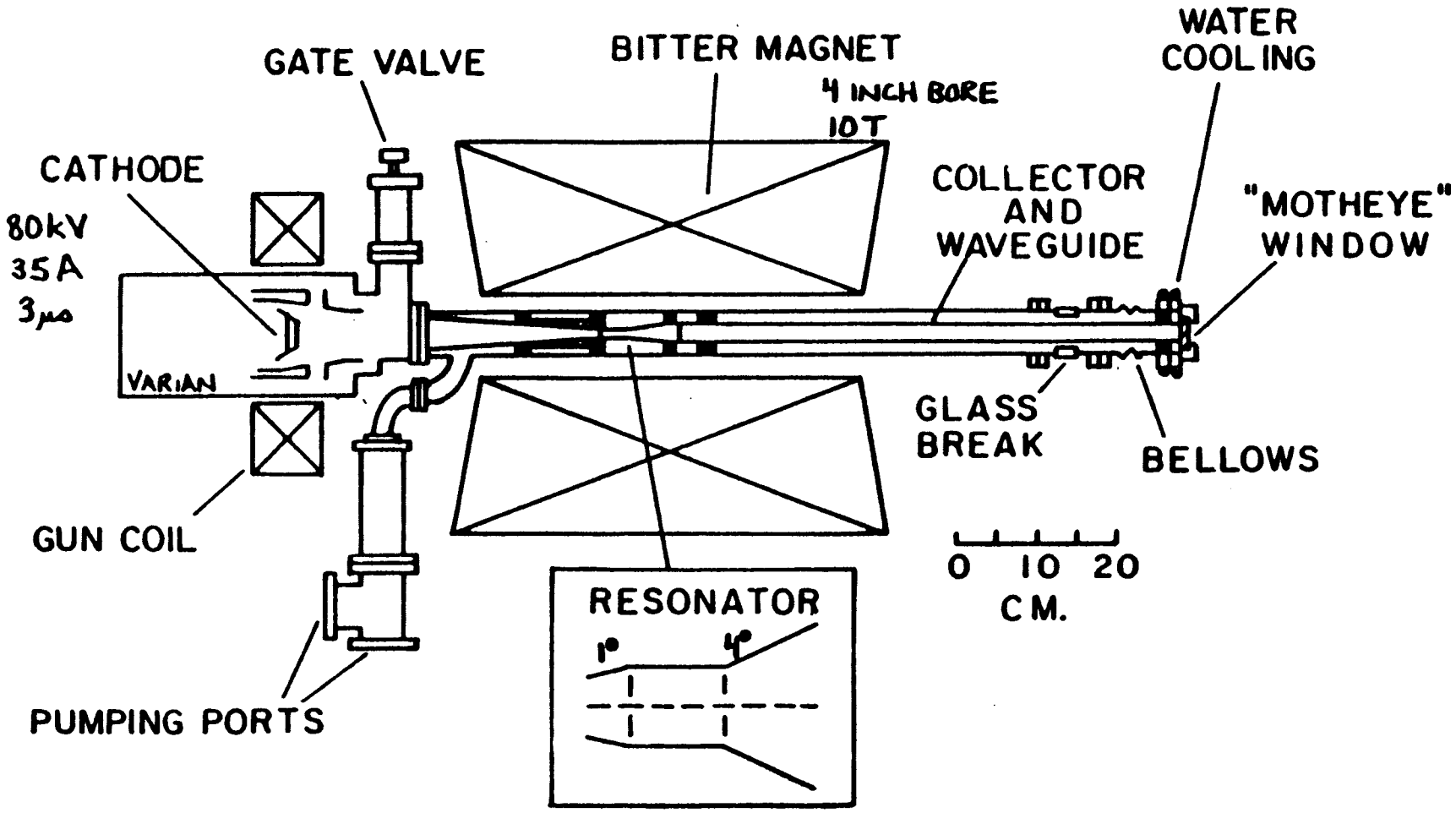

Figure 1

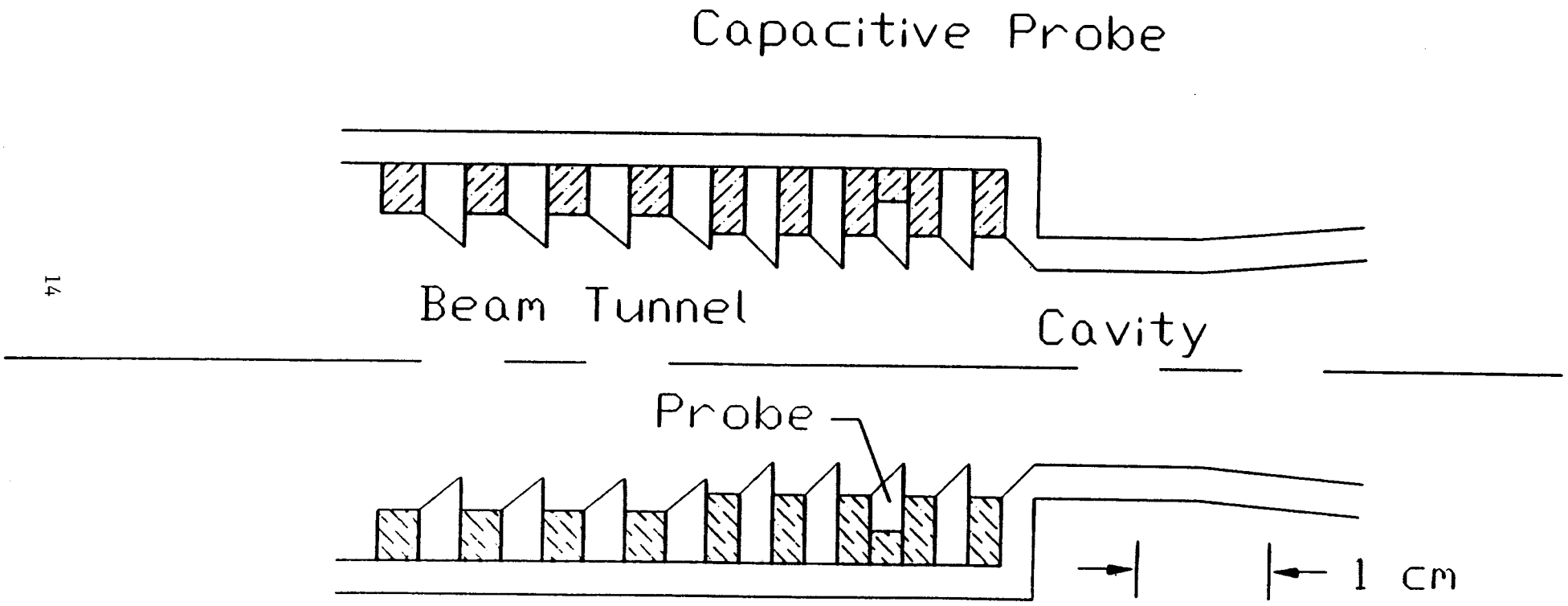

Figure 2

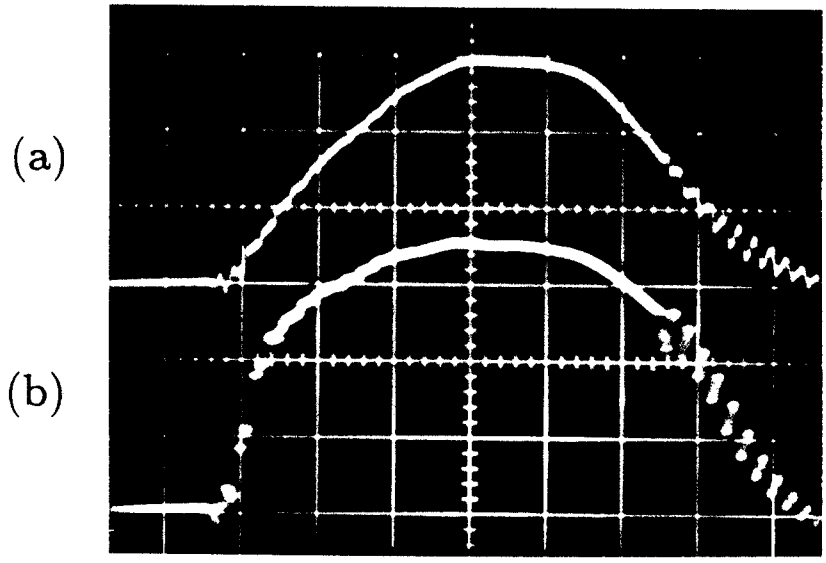

Figure 3

(a)

(b)

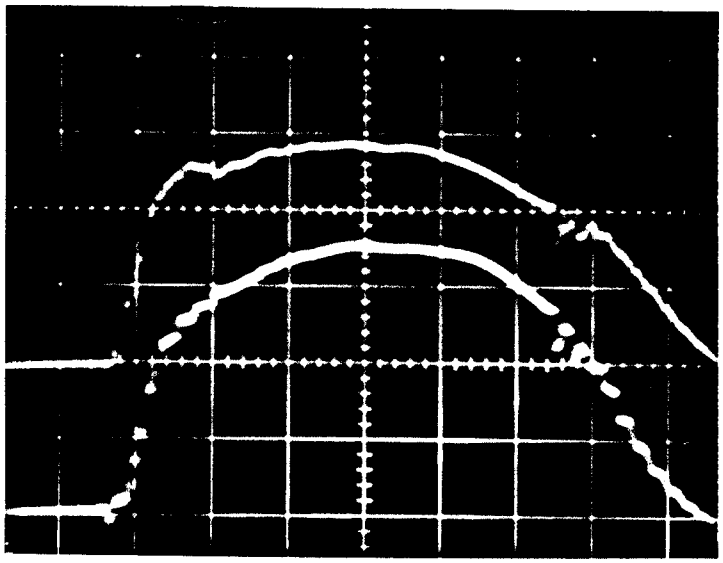

Figure 4

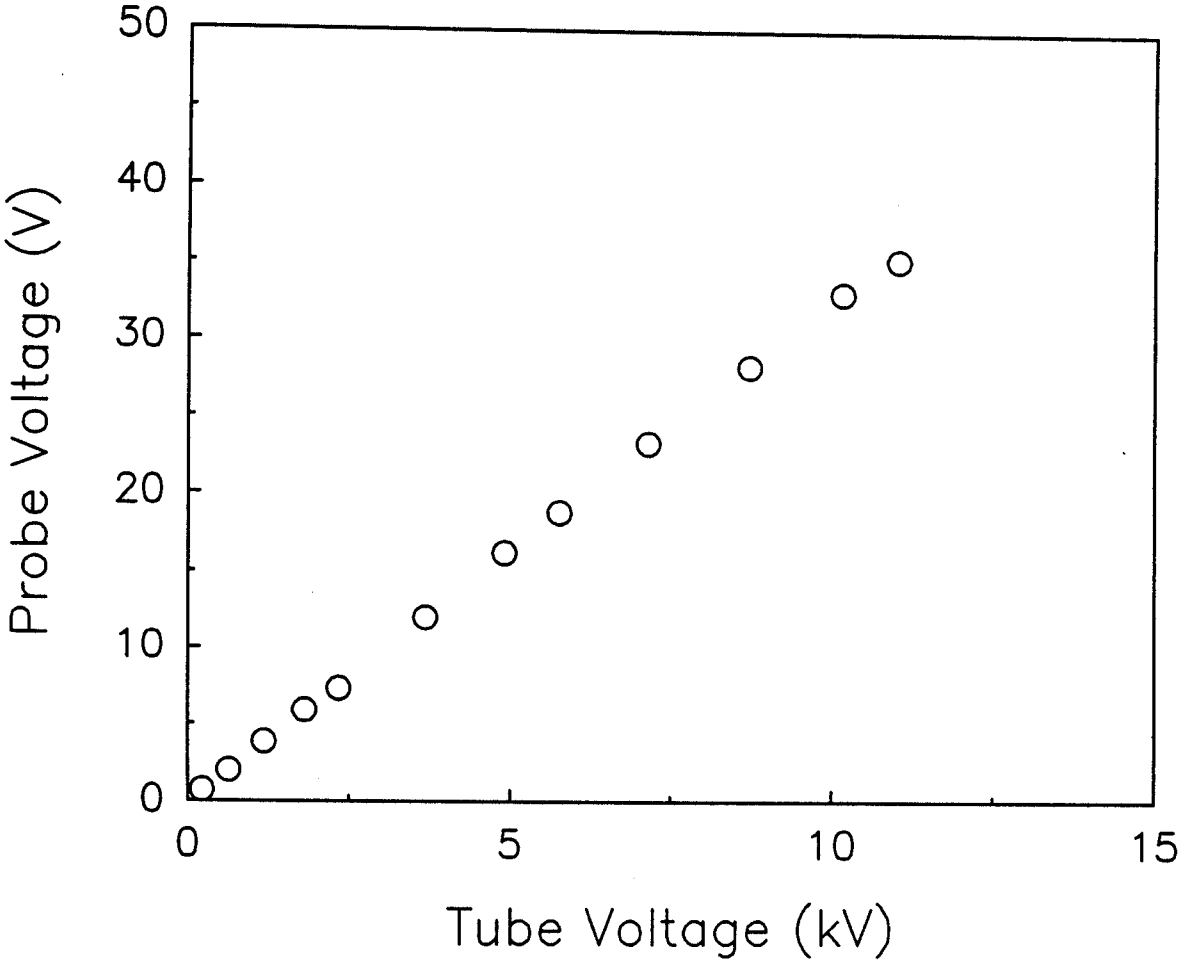

Figure 5

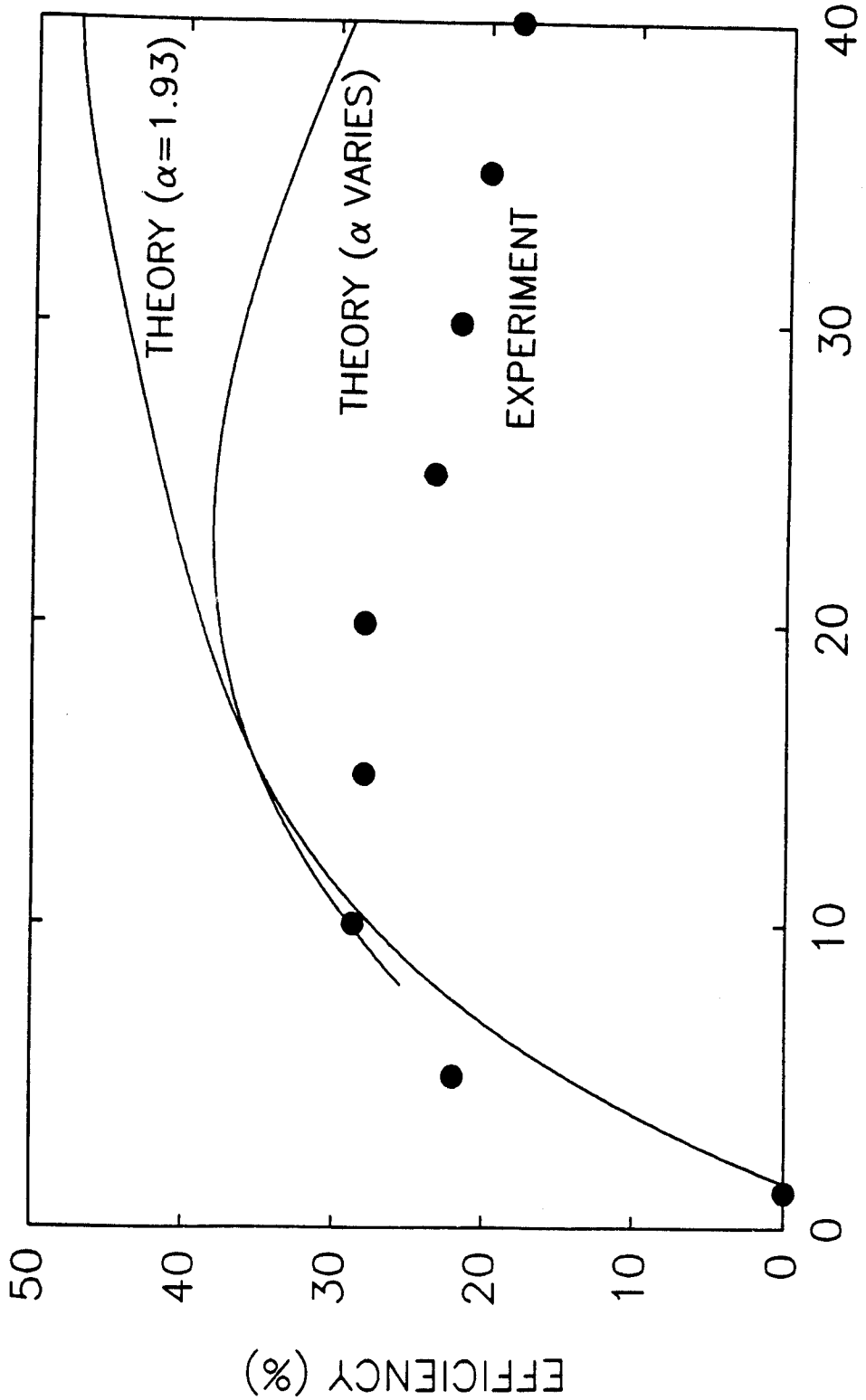
EFFICIENCY (%)
50
40
30
20
10
0
0
10
20
30
40
BEAM CURRENT (A)
THEORY (α=1.93)
THEORY (α VARIES)
EXPERIMENT

Figure 6

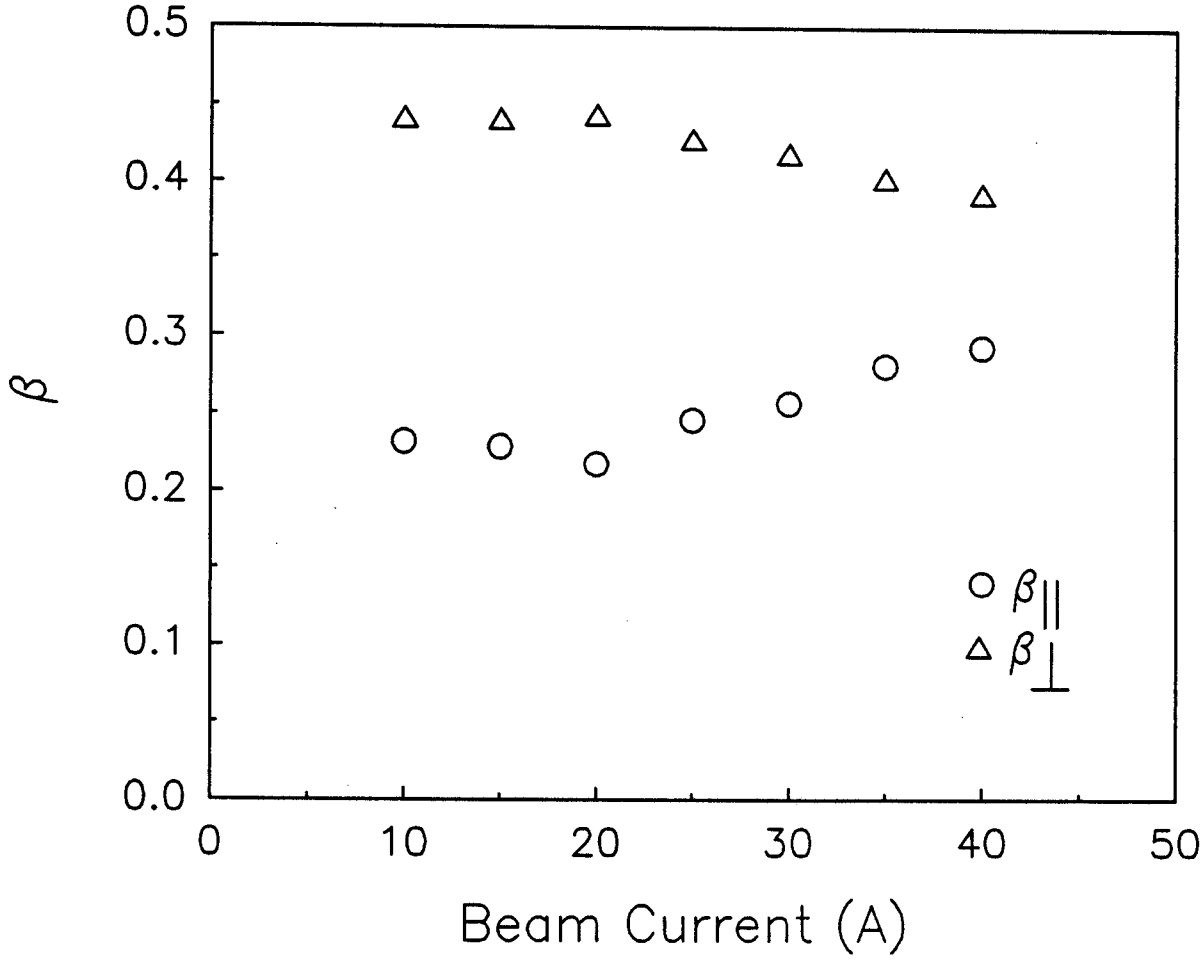

Figure 7

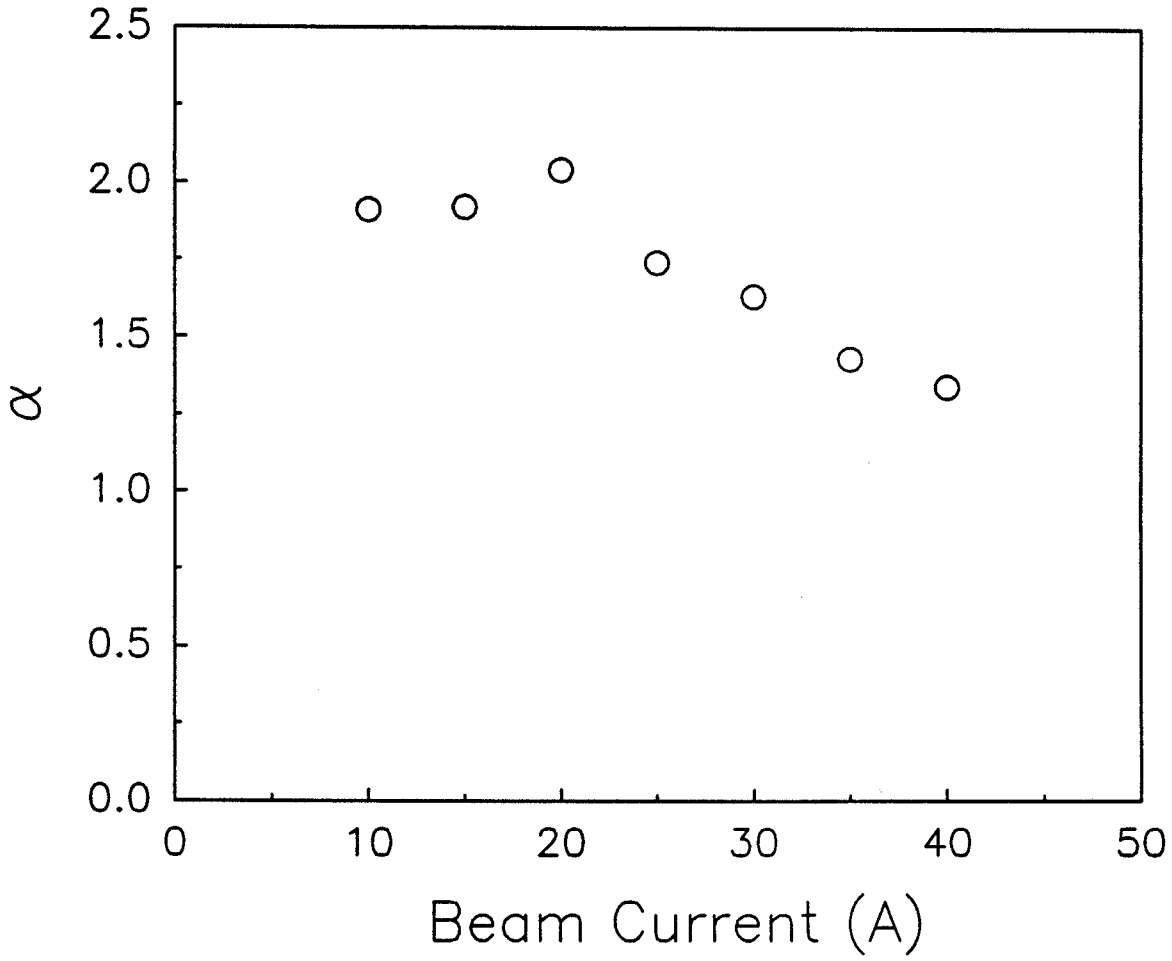

Figure 8

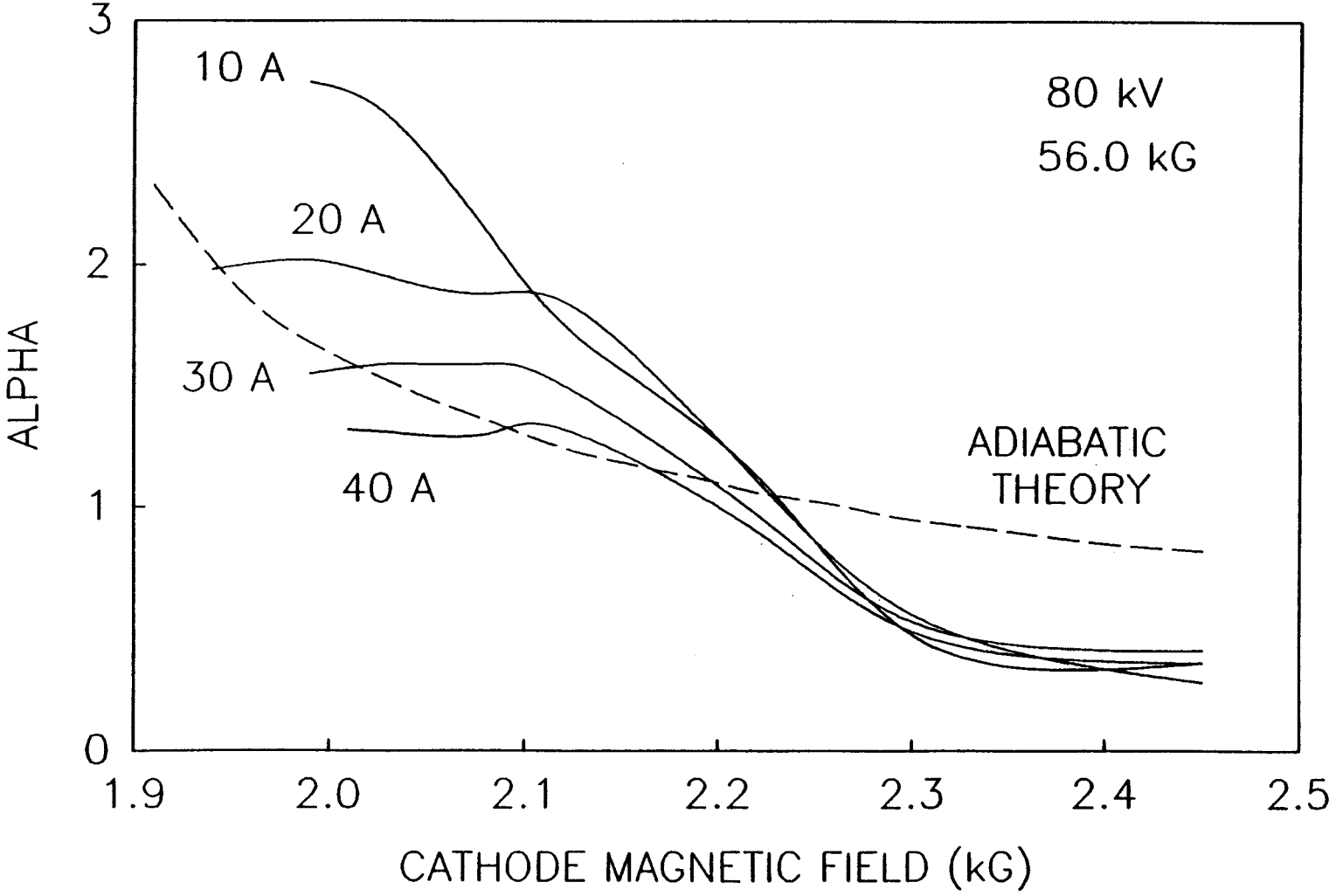
3
2
1
0
ALPHA
10 A
20 A
30 A
40 A
80 kV
56.0 kG
ADIABATIC
THEORY
1.9
2.0
2.1
2.2
2.3
2.4
2.5
CATHODE MAGNETIC FIELD (kG)

Figure 9

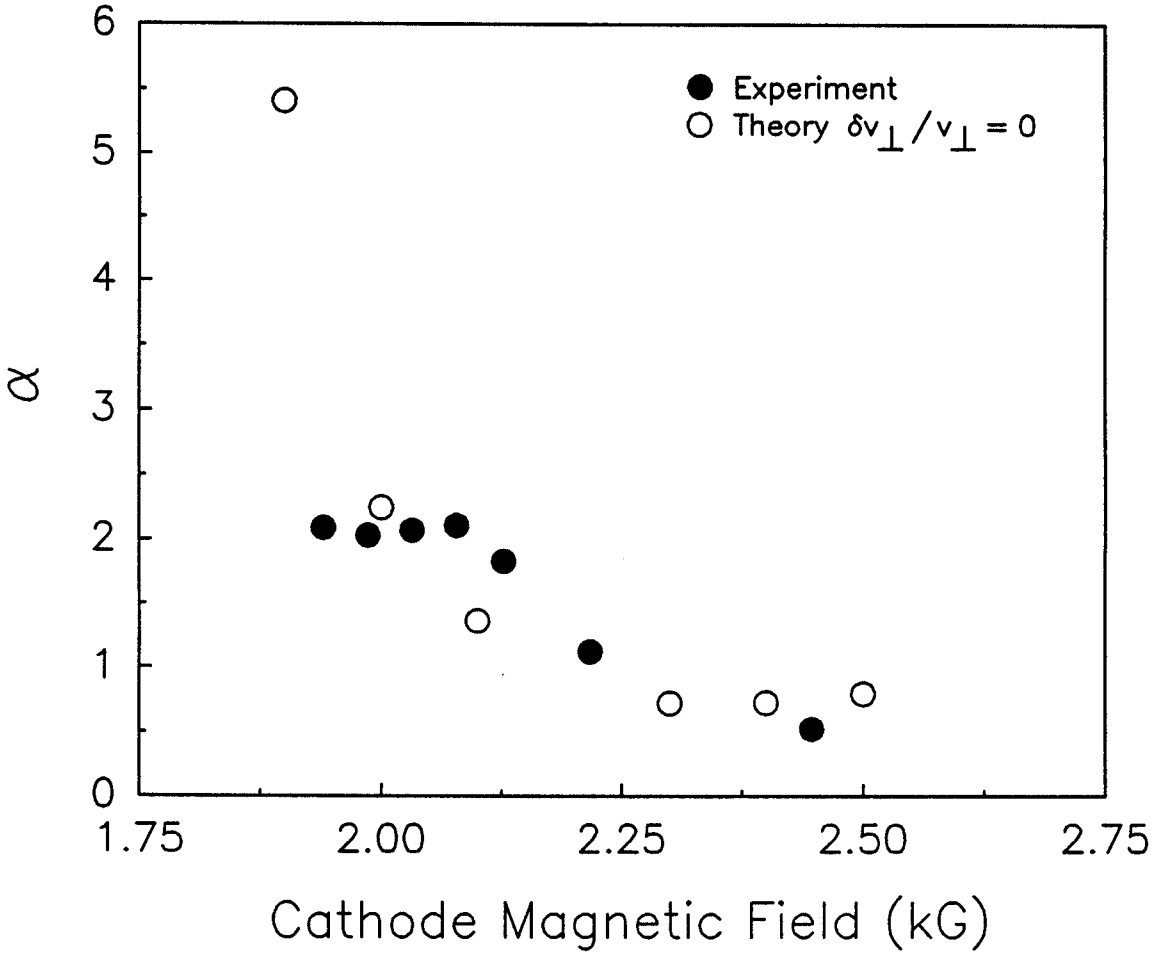
Experiment
Theory $\delta v_\perp / v_\perp = 0$
α
0
1
2
3
4
5
6
1.75
2.00
2.25
2.50
2.75
Cathode Magnetic Field (kG)

Figure 10

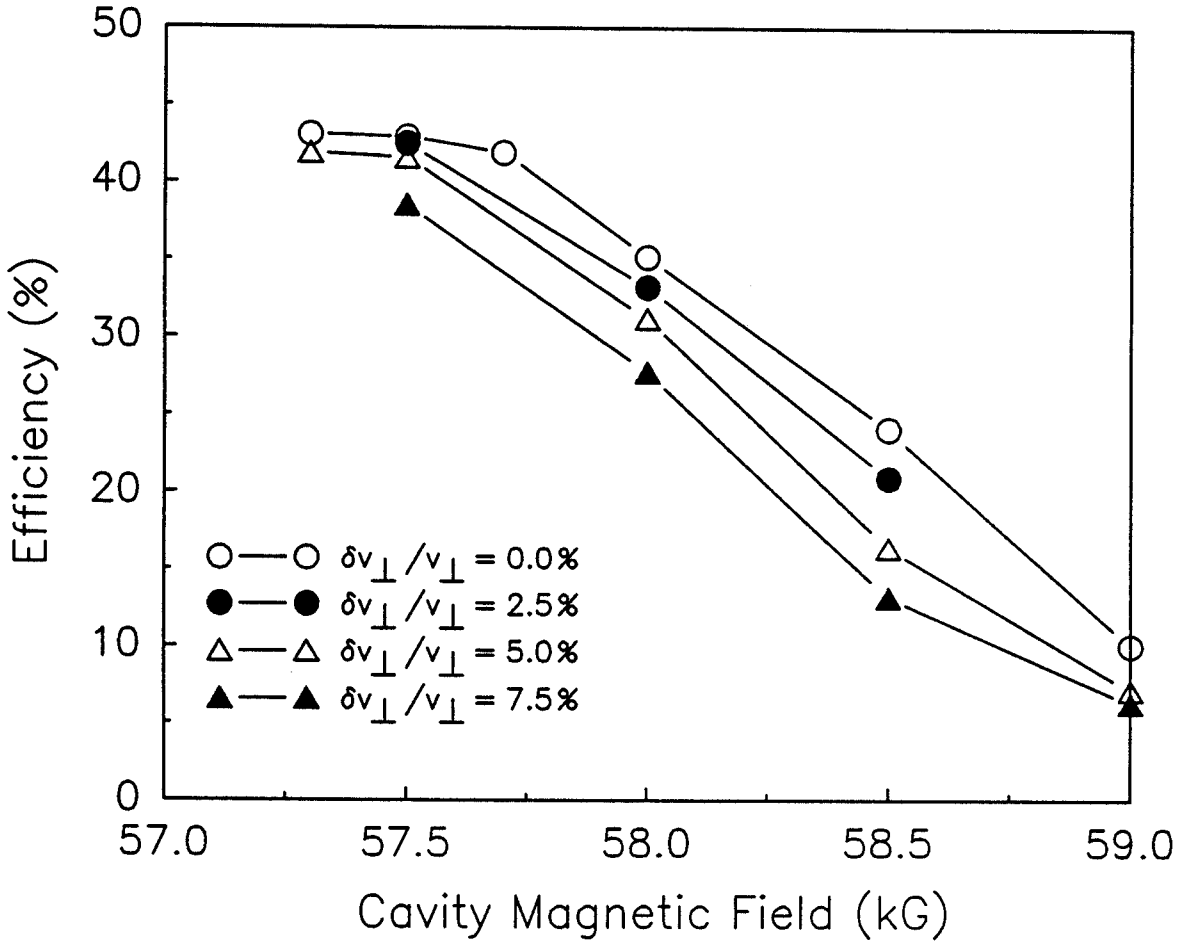
50
40
30
20
10
0
Efficiency (%)
57.0
57.5
58.0
58.5
59.0
Cavity Magnetic Field (kG)
δv⊥ /v⊥ = 0.0%
δv⊥ /v⊥ = 2.5%
δv⊥ /v⊥ = 5.0%
δv⊥ /v⊥ = 7.5%

Figure 11

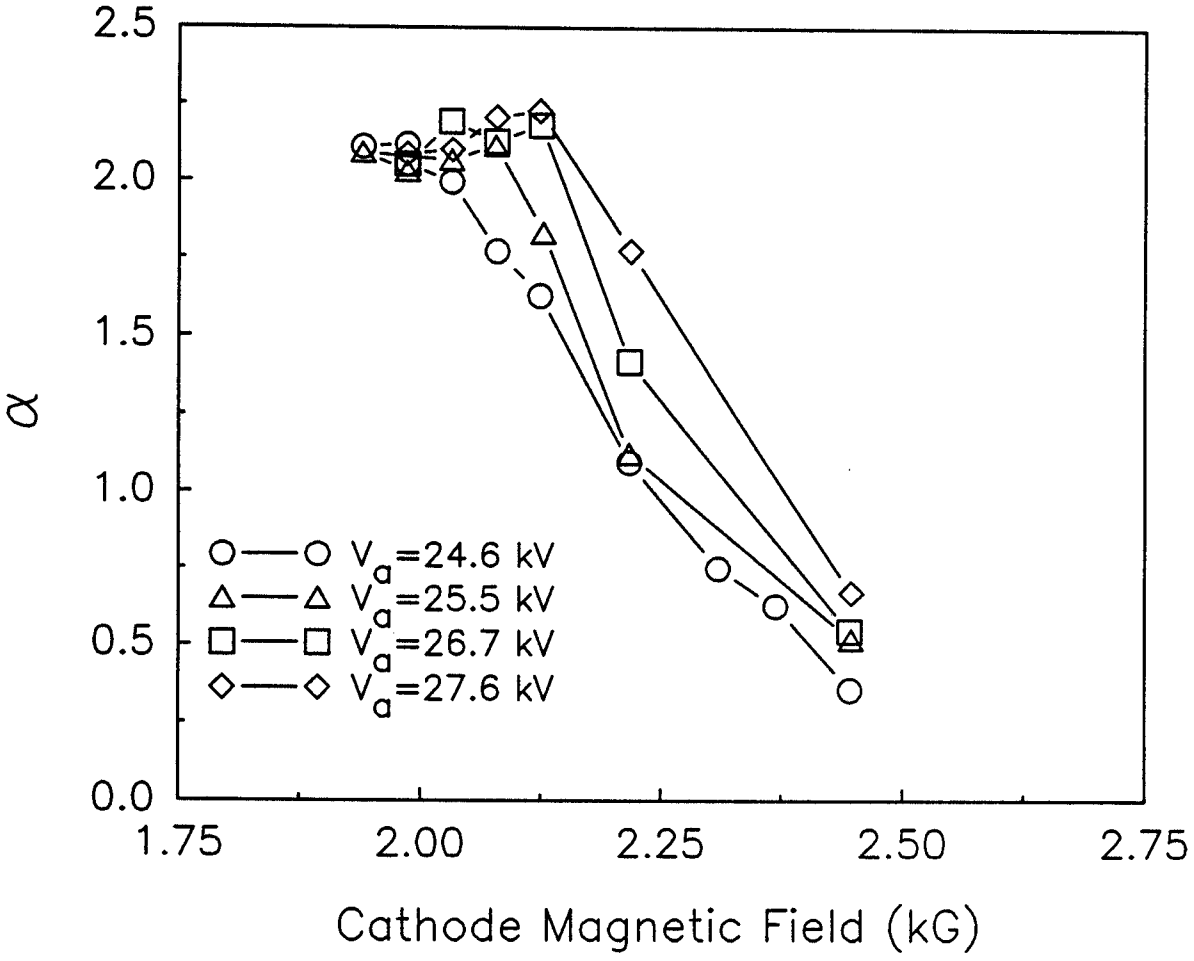
2.5
2.0
1.5
1.0
0.5
0.0
α
1.75
2.00
2.25
2.50
2.75
Cathode Magnetic Field (kG)
V_a=24.6 kV
V_a=25.5 kV
V_a=26.7 kV
V_a=27.6 kV

Figure 12